Practical GFDM-based Linear Receivers

Ahmad Nimr*, Marwa Chafii[†], Gerhard Fettweis*

*Vodafone Chair Mobile Communication Systems, Technische Universität Dresden, Germany

† ETIS UMR 8051, Université Paris Seine, Université de Cergy-Pontoise, ENSEA, CNRS, France
ahmad.nimr@ifn.et.tu-dresden.de, marwa.chafii@ensea.fr, gerhard.fettweis@tu-dresden.de

Abstract—The conventional receiver designs of generalized frequency division multiplexing (GFDM) consider a large scale multiple-input multiple-output (MIMO) system with a block circular matrix of combined channel and modulation. Exploiting this structure, several approaches have been proposed for low complexity joint linear minimum mean squared error (LMMSE) receiver. However, the joint design is complicated and inappropriate for hardware implementation. In this paper, we define the concept of GFDM-based linear receivers, which first performs channel equalization (CEq) and afterwards the equalized signal is processed with GFDM demodulator. We show that the optimal joint LMMSE receiver is equivalent to a GFDM-based one, that applies LMMSE-CEq and zero-forcing demodulation. For orthogonal modulation, the optimal LMMSE receiver has an implementation-friendly structure. For the non-orthogonal case, we propose two practical designs that approach the performance of the joint LMMSE. Finally, we analytically prove that GFDMbased receivers achieve equal signal-to-interference-plus-noise ratio per subsymbols within the same subcarrier.

Index Terms—Equalization, GFDM, LMMSE, low-complexity

I. INTRODUCTION

In its early proposal, generalized frequency division multiplexing (GFDM) [1] has been suggested as an alternative to orthogonal frequency division multiplexing (OFDM). Recently, GFDM has been extended to a multicarrier framework, that is able to process most of the state of the art waveforms and allows the design of new waveforms [2]. The welldefined structure of GFDM enables a feasible real-time modem implementation on hardware. For instance the approaches in [3] and [4] provide implementations in the time domain (TD) and frequency domain (FD), respectively. However, the low complexity receiver approaches in fading channels practically consider zero-forcing (ZF)-channel equalization (CEq). One of the main objectives of conventional GFDM is providing low out-of-band (OOB). This requires a design of the prototype pulse with subcarrier overlapping leading to a non-orthogonal modulation [5]. As a consequence, tackling the self intersymbol-interference (ISI) and inter-carrier-interference (ICI) at the receiver becomes challenging in the design of the GFDM receiver. By exploiting the sparse representation of the FD pulse shape, an interference cancellation approach is proposed in [6]. In that work, after ZF-CEq, and matched filter (MF) demodulation, the ICI in a subcarrier is canceled

The work presented in this paper has been performed in the framework of the ORCA project [https://www.orca-project.eu/]. This project has received funding from the European Union's Horizon 2020 research and innovation programme under grant agreement No 732174.

based on the hard decision estimation of the symbols from the adjacent subcarriers. Joint linear minimum mean squared error (LMMSE) receiver has been widely studied considering a large scale multiple-input multiple-output (MIMO) matrix. The computation of the LMMSE filter is complex, especially for hardware implementation. By exploiting the block diagonal structure of the equivalent MIMO channel, the algorithm in [7] reduces the complexity of computing the LMMSE filter from a cubic to square order. However, the receiver needs to compute the inverse of smaller-scale matrices. The works in [8] and [9] reproduce the same results by means of the decomposition of the modulation matrix. A special low-complexity order is given in [8] for orthogonal modulation matrix. Nevertheless, the latter approaches focus more on the theoretical analysis of the performance without the consideration of hardware implementation. The joint LMMSE performance in terms of uncoded bit error rate (BER) is studied in [10] via a closed-form approximation using the achieved signal-to-interference-plusnoise ratio (SINR) per symbol. However, a low-complexity computation of the SINR is missing in that work.

In this paper, we aim at a practical implementation of linear GFDM receivers via decoupled CEq and demodulation. We refer to this type of receivers as GFDM-based receivers. By means of two-dimensional representation, we show that the received signal in frequency selective channels consists of M parallel uncorrelated small-scale signals. Accordingly, the GFDM-based receiver as well as the SINRs of the demodulated symbols are analytically computed. We show that GFDM-based receivers achieve equal-SINR per subsymbols within the same subcarrier. The optimal joint LMMSE is equivalent to LMMSE-CEq and ZF demodulation. For an orthogonal modulation matrix, the LMMSE-CEq requires to compute the inverse of a diagonal matrix. In the nonorthogonal case, we show that the CEq can be performed on small-scale parallel signals. Moreover, a low-complexity practical approximation of LMMSE-CEq is derived. Furthermore, we investigate the LMMSE demodulation after ZF-CEq. Both approximations approach the performance of the optimal joint LMMSE, while allowing a practical implementation

The remainder of the paper is organized as follows: Section II introduces the system model and an overview of GFDM FD modem structure. Section III is dedicated for the design of GFDM-based receivers. In Section IV, we focus on the parallel system model which is used to analytically drive the receivers and the SINR expressions. Section V provides numerical results. Finally, Section VI concludes the paper.

II. SYSTEM MODEL

We consider a GFDM system with K subcarriers, M subsymbols, and a prototype pulse g[n]. The GFDM block $x \in \mathbb{C}^{N \times 1}$, N = KM, is given by [1]

$$[\mathbf{x}]_{(n)} = \sum_{k=0}^{K-1} \sum_{m=0}^{M-1} [\mathbf{D}]_{(k,m)} g[\langle n - mK \rangle_N] e^{j2\pi \frac{k}{K}n}, \quad (1)$$

where $\langle \cdot \rangle_N$ is the modulo-N operator and $\mathbf{D} \in \mathbb{C}^{K \times M}$ is the input data matrix. The data symbol $d_{k,m} = [\mathbf{D}]_{(k,m)}$ is transmitted on the m-th subsymbol of the k-th subcarrier. The GFDM block can be expressed in a matrix notation as

$$x = Ad$$
, $[A]_{(n,k+mK)} = g[\langle n - mK \rangle_N]e^{j2\pi \frac{kn}{K}}$, (2)

where $d = \text{vec}\{D\}$. A frame of GFDM blocks is transmitted over block fading wireless multipath channel with impulse response h[l]. To enable FD equalization, a cyclic prefix (CP) longer than the channel delay spread is appended to the beginning of each GFDM block. After removing the CP, we get the received block y = HAd + v, where $H \in \mathbb{C}^{N \times N}$ is the circular channel matrix, $[H]_{(n,q)} = h[< n - q >_N]$. The additive white Gaussian noise (AWGN) vector with variance σ^2 is denoted as v. By applying N-discrete Fourier transform (DFT), the FD received block is written as

$$\tilde{\mathbf{y}} = \mathbf{\Lambda}^{(\tilde{h})} \tilde{\mathbf{A}} \mathbf{d} + \tilde{\mathbf{v}},\tag{3}$$

where $\mathbf{\Lambda}^{(\tilde{h})} = \operatorname{diag}\left\{\{\left[\tilde{\boldsymbol{h}}\right]_{(n)}\}_{n=0}^{N-1}\right\}$ is the equivalent FD diagonal channel matrix, $\boldsymbol{h} = N\text{-DFT}\{h[l]\}$. The notation $\tilde{\boldsymbol{X}} = \boldsymbol{F}_N \boldsymbol{X}$ denotes the N-DFT of the columns of \boldsymbol{X} .

A. Joint receiver

This approach considers the general MIMO system [9]

$$\tilde{y} = \boldsymbol{H}^{(\text{eff})} \boldsymbol{d} + \tilde{\boldsymbol{v}}, \ \boldsymbol{H}^{(\text{eff})} = \boldsymbol{\Lambda}^{(\tilde{h})} \tilde{\boldsymbol{A}}.$$
 (4)

All the approaches of MIMO receiver can be applied. The structure of \tilde{A} can be exploited for low complexity computation. For instance, the joint ZF $(H^{(\text{eff})-1})$ is decoupled into ZF-CEq $(\Lambda^{(\tilde{h})}^{-1})$ and ZF-GFDM-demodulator (\tilde{A}^{-1}) . Moreover, assuming uncorrelated data, i.e. $R_d = \mathbb{E}\left[dd^H\right] = E_s I_N$, where E_s is the average symbol power, and $R_{\tilde{v}} = \mathbb{E}\left[\tilde{v}\tilde{v}^H\right] = \tilde{\sigma}^2 I_N$, $\tilde{\sigma}^2 = N\sigma^2$, the LMMSE receiver filter is given by

$$\boldsymbol{W}^{H} = \boldsymbol{H}^{(\text{eff})H} \left(\boldsymbol{H}^{(\text{eff})} \boldsymbol{H}^{(\text{eff})H} + \frac{\tilde{\sigma}^{2}}{E_{s}} \boldsymbol{I}_{N} \right)^{-1}.$$
 (5)

In the case of orthogonal modulation matrix, i.e. $AA^H = I_N \Rightarrow \tilde{A}\tilde{A}^H = NI_N$, the joint LMMSE is reduced to

$$\boldsymbol{W}^{H} = \frac{1}{N} \tilde{\boldsymbol{A}}^{H} \underbrace{\boldsymbol{\Lambda}^{(\tilde{h})}^{H} \left(\boldsymbol{\Lambda}^{(\tilde{h})} \boldsymbol{\Lambda}^{(\tilde{h})}^{H} + \frac{\tilde{\sigma}^{2}}{E_{s}} \boldsymbol{I}_{N}\right)^{-1}}_{\boldsymbol{\Lambda}_{eq}^{(\tilde{h})}}.$$
 (6)

This can be computed by first performing CEq with the matrix $\Lambda_{\rm eq}^{(\tilde{h})}$ and then MF-GFDM-demodulation. In this case, the LMMSE implementation is feasible. On the contrary, when \boldsymbol{A} is non-orthogonal, the hardware realization of the joint LMMSE is not affordable.

B. Frequency-domain modem

Fig. 1: GFDM FD modem, the highlighted box represents (9).

The structure of the FD modulation matrix \tilde{A} is derived from the FD block representation

$$[\tilde{x}]_{(n)} = \sum_{m=0}^{M-1} \sum_{k=0}^{K-1} [\mathbf{D}]_{(k,m)} \, \tilde{g}[\langle n - kM \rangle_N] e^{-j2\pi \frac{m}{M}n}.$$
 (7)

Here, $\tilde{g}[n]$ is the FD prototype pulse. By reformulating (7) using two indexes $p=0,\cdots,M-1$ and $q=0,\cdots,K-1$, with n=p+qM, we get

$$[\tilde{x}]_{(p+qM)} = \sum_{k=0}^{K-1} \tilde{g}[\langle p + [q-k]M \rangle_N] \sum_{m=0}^{M-1} [\mathbf{D}]_{(k,m)} e^{-j2\pi \frac{mp}{M}}.$$

The matrix notation $V_{K,M}^{(\tilde{x})} \in \mathbb{C}^{K \times M}$ is defined such that

$$\left[\boldsymbol{V}_{K,M}^{(\tilde{\boldsymbol{x}})}\right]_{(q,p)} = \left[\tilde{\boldsymbol{x}}\right]_{(p+qM)} \Leftrightarrow \boldsymbol{V}_{K,M}^{(\tilde{\boldsymbol{x}})} = \text{unvec}_{M \times K} \left\{\tilde{\boldsymbol{x}}\right\}^{T}. \quad (8)$$

Thus,
$$\left[oldsymbol{V}_{K,M}^{(ilde{oldsymbol{x}})} \right]_{(q,p)} = \sum_{k=0}^{K-1} \left[oldsymbol{V}_{K,M}^{(ilde{oldsymbol{g}})} \right]_{(< q-k>_K,p)} \left[oldsymbol{D} oldsymbol{F}_M
ight]_{(k,p)}.$$

This defines a circular convolution between the p-th column of $V_{K,M}^{(\bar{g})}$ and the p-th column of DF_M . Accordingly,

$$\boldsymbol{V}_{K,M}^{(\tilde{\boldsymbol{x}})} = \boldsymbol{V}_{K,M}^{(\tilde{\boldsymbol{g}})} \circledast_1 [\boldsymbol{D}\boldsymbol{F}_M], \tag{9}$$

where \circledast_1 denotes the circular convolution with respect to the first dimension, i.e. the columns. This circular convolution can be expressed using K-IDFT as

$$\begin{bmatrix} \boldsymbol{F}_{K}^{H} \boldsymbol{V}_{K,M}^{(\tilde{\boldsymbol{x}})} \end{bmatrix}_{(q,p)} = \begin{bmatrix} \boldsymbol{F}_{K}^{H} \boldsymbol{V}_{K,M}^{(\tilde{\boldsymbol{g}})} \end{bmatrix}_{(q,p)} \begin{bmatrix} \boldsymbol{F}_{K}^{H} \boldsymbol{D} \boldsymbol{F}_{M} \end{bmatrix}_{(q,p)}.$$
Therefore, $\boldsymbol{V}_{K,M}^{(\tilde{\boldsymbol{x}})} = \boldsymbol{F}_{K} \left(\boldsymbol{W}_{\text{tx}} \odot \begin{bmatrix} \frac{1}{K} \boldsymbol{F}_{K}^{H} \boldsymbol{D} \boldsymbol{F}_{M} \end{bmatrix} \right).$ (10)

Here, \odot denotes the element-wise multiplication operator, and W_{tx} is the modulator window, which is derived from \tilde{g} as

$$\boldsymbol{W}_{\mathrm{tx}} = \boldsymbol{F}_{K}^{H} \boldsymbol{V}_{K,M}^{(\tilde{\boldsymbol{g}})} \in \mathbb{C}^{K \times M}. \tag{11}$$

Fig. 1 illustrates the block diagram of the FD modem. The highlighted box corresponds to the convolution (9). The FD demodulator performs the inverse operations on the FD equalized block \tilde{y}_{eq} using a receiver window W_{rx} ,

$$\hat{\boldsymbol{D}} = \frac{1}{M} \boldsymbol{F}_K \left(\boldsymbol{W}_{\text{rx}} \odot \left[\frac{1}{K} \boldsymbol{F}_K^H \boldsymbol{V}_{K,M}^{(\tilde{\boldsymbol{y}}_{\text{eq}})} \right] \right) \boldsymbol{F}_M^H.$$
 (12)



Fig. 2: GFDM baseband system model.

C. GFDM matrix structure

The structure of $\tilde{\boldsymbol{A}}$ can be revealed by the vectorization of (10), where $\tilde{\boldsymbol{x}} = \operatorname{vec}\left\{\boldsymbol{V}_{K,M}^{(\tilde{\boldsymbol{x}})}\right\} = \tilde{\boldsymbol{A}}\boldsymbol{d}$. As a result

$$\tilde{A} = \underbrace{\Pi_{K,M} U_{M,K}}_{V_f} \Lambda^{(tx)} \underbrace{U_{M,K}^H \Pi_{M,K} U_{K,M} \Pi_{K,M}}_{U_t}.$$
 (13)

Here $\Pi_{Q,P}$ is the commutative matrix of size $QP \times QP$ defined such that for a matrix $\boldsymbol{X} \in \mathbb{C}^{Q \times P}$, $\operatorname{vec} \left\{ \boldsymbol{X}^T \right\} = \Pi_{Q,P} \operatorname{vec} \left\{ \boldsymbol{X} \right\}$, $\boldsymbol{U}_{P,Q}$ is unitary matrix given by $\boldsymbol{U}_{P,Q} = \frac{1}{\sqrt{Q}} \boldsymbol{I}_P \otimes \boldsymbol{F}_Q$, and $\boldsymbol{\Lambda}^{(\mathrm{tx})}$ is a diagonal matrix given by

$$\mathbf{\Lambda}^{(\mathsf{tx})} = \sqrt{M} \operatorname{diag} \left\{ \operatorname{vec} \left\{ \mathbf{W}_{\mathsf{tx}} \right\} \right\}. \tag{14}$$

Note that V_f and U_t are unitary matrices. Hence, we define

Definition 1. An FD GFDM matrix of K subcarriers and M subsymbols is a square matrix of size $N \times N$ that can be decomposed according to (13).

From the demodulator structure, the FD demodulator matrix $\tilde{B} \in \mathbb{C}^{N \times N}$, where $\hat{d} = \tilde{B}^H \tilde{y}_{eq}$ is a GFDM matrix given by

$$\tilde{\boldsymbol{B}} = \underbrace{\boldsymbol{\Pi}_{K,M} \boldsymbol{U}_{M,K}}_{\boldsymbol{V}_f} \boldsymbol{\Lambda}^{(rx)H} \underbrace{\boldsymbol{U}_{M,K}^H \boldsymbol{\Pi}_{M,K} \boldsymbol{U}_{K,M} \boldsymbol{\Pi}_{K,M}}_{\boldsymbol{U}_t}. \tag{15}$$
Here,
$$\boldsymbol{\Lambda}^{(rx)} = \frac{1}{\sqrt{M}} \operatorname{diag} \left\{ \operatorname{vec} \left\{ \boldsymbol{W}_{rx} \right\} \right\}.$$

The design of the demodulator is achieved by computing the diagonal matrix $\Lambda^{(rx)}$ or equivalently the window W_{rx} .

III. GFDM-BASED RECEIVER

In a realistic implementation of GFDM receiver, a CEq precedes the demodulation. Usually a simple ZF-CEq is applied [3]. By considering independent designs of the CEq and demodulation, we formulate the following definition:

Definition 2. A GFDM-based receiver is a receiver that first, performs CEq, and then, the equalized signal is demodulated with a GFDM demodulator.

This definition can be applied for TD or FD processing. In this work, we focus on FD GFDM-based receiver. Namely, an FD channel equalizer and FD demodulator as illustrated in Fig. 2.

A. Relation to joint LMMSE receiver

The relation between a GFDM-based receiver and the joint LMMSE receiver is summarized by the following lemma:

Lemma 1. If $\Lambda^{(\tilde{h})}$, \tilde{A} are invertible, and the data and noise are uncorrelated, such that $\mathbf{R}_d = E_s \mathbf{I}_N$, and $\mathbf{R}_{\tilde{v}} = \tilde{\sigma}^2 \mathbf{I}_N$, the LMMSE receiver can be computed in two ways:

- 1) LMMSE-CEq on the linear model $\tilde{y}_{eq} = \Lambda^{(\tilde{h})} \tilde{x} + v$, $R_{\tilde{x}} = E_s \tilde{A} \tilde{A}^H$ followed by ZF demodulation, $\hat{d} = \tilde{A}^{-1} \tilde{y}_{eq}$.
- 2) ZF-CEq, i.e. $\tilde{y}_{eq} = {\Lambda^{(\tilde{h})}}^{-1} y$, followed by LMMSE demodulation on $\tilde{y}_{eq} = \tilde{A}d + \bar{v}$, $R_{\bar{v}} = \tilde{\sigma}^2 \left[{\Lambda^{(\tilde{h})} {\Lambda^{(\tilde{h})}}^H} \right]^{-1}$.

The proof is given in Appendix A. The first method, represents a decoupled LMMSE-CEq,

$$\tilde{\boldsymbol{H}}_{\text{LMMSE}}^{H} = \left(\boldsymbol{\Lambda}^{\left(\tilde{h}\right)}{}^{H}\boldsymbol{\Lambda}^{\left(\tilde{h}\right)} + \frac{\tilde{\sigma}^{2}}{E_{s}}\left[\tilde{\boldsymbol{A}}\tilde{\boldsymbol{A}}^{H}\right]^{-1}\right)^{-1}\boldsymbol{\Lambda}^{\left(\tilde{h}\right)}{}^{H}, \quad (16)$$

followed by a ZF-GFDM-demodulation with the demodulator window $[W_{\rm rx}]_{(k,m)} = \left[[W_{\rm tx}]_{(k,m)} \right]^{-1}$. This case follows the definition of a GFDM-based receiver. If $R_{\tilde{x}}$ is diagonal, e.g. when A is orthogonal, the LMMSE-CEq is reduced to the computation of the inverse of a diagonal matrix, which is simple for realization. Otherwise, the main complexity is inherited from the computation of the inverse $\left(\Lambda^{(\tilde{h})}^H \Lambda^{(\tilde{h})} + \frac{\tilde{\sigma}^2}{E_s} \left[\tilde{A} \tilde{A}^H \right]^{-1} \right)$. However, a reduced complexity can be achieved using the decomposition of (13), where $\left[\tilde{A} \tilde{A}^H \right]^{-1} = V_f \left[\Lambda^{({\rm tx})} \Lambda^{({\rm tx})H} \right]^{-1} V_f^H$. This allows the computation of $\tilde{H}_{\rm LMMSE}^H$ using the inverse of M matrices each of size $K \times K$ as derived in [7]. We provide a simplified derivation in Section IV-A. In the second approach, the LMMSE demodulation following ZF-CEq is given by

$$B_{\text{MMSE}}^{H} = \tilde{A}^{H} \left(\tilde{A} \tilde{A}^{H} + \frac{\tilde{\sigma}^{2}}{E_{s}} R_{\bar{v}} \right)^{-1}$$

$$= U_{t}^{H} \underbrace{\Lambda^{(\text{tx})H} \left(\Lambda^{(\text{tx})} \Lambda^{(\text{tx})H} + V_{f}^{H} \frac{R_{\bar{v}}}{E_{s}} V_{f} \right)^{-1}}_{\Gamma^{(\text{rx})}} V_{f}^{H}.$$
(17)

If the matrix $\Gamma^{(rx)}$ is diagonal, e.g. AWGN [4] channel, then $B_{\rm MMSE}$ becomes a GFDM matrix. Otherwise, $B_{\rm MMSE}^H$ cannot be implemented with GFDM-demodulator. Nevertheless, the demodulator can be designed with LMMSE under the constraint of GFDM matrix, as discussed in Section IV-B.

IV. GFDM PARALLEL SIGNAL MODEL

Using (9) and (8), the received signal can be represented as

$$V_{K,M}^{(\tilde{\mathbf{y}})} = V_{K,M}^{(\tilde{\mathbf{h}})} \odot \left(V_{K,M}^{(\tilde{\mathbf{g}})} \circledast_1 [\mathbf{D}\mathbf{F}_M] \right) + V_{K,M}^{(\tilde{\mathbf{v}})}.$$
(18)

As illustrated in Fig. 3, the m-th column, $\tilde{\pmb{y}}_m = \left[\pmb{V}_{K,M}^{(\tilde{\pmb{y}})} \right]_{(:,m)}$, can be written in the form

$$\tilde{\boldsymbol{y}}_{m} = \boldsymbol{\Lambda}_{m}^{(\tilde{h})} \tilde{\boldsymbol{A}}_{m} \tilde{\boldsymbol{d}}_{m} + \tilde{\boldsymbol{v}}_{m}, \tilde{\boldsymbol{v}}_{m} = \left[\boldsymbol{V}_{K,M}^{(\tilde{v})} \right]_{(\cdot m)} \in \mathbb{C}^{K \times 1}, \quad (19)$$

where, $\tilde{\boldsymbol{d}}_m = [\boldsymbol{D}\boldsymbol{F}_M]_{(:,m)}$, $\boldsymbol{\Lambda}_m^{(\tilde{h})} = \operatorname{diag}\left\{\left[\boldsymbol{V}_{K,M}^{(\tilde{h})}\right]_{(:,m)}\right\}$, and $\tilde{\boldsymbol{A}}_m \in \mathbb{C}^{K \times K}$ is a circular matrix generated from the column vector $\tilde{\boldsymbol{g}}_m = \left[\boldsymbol{V}_{K,M}^{(\tilde{\boldsymbol{g}})}\right]_{(:,m)}$. It can be expressed by means of K-DFT and the modulator window (11) as

$$\tilde{\boldsymbol{A}}_{m} = \frac{1}{K} \boldsymbol{F}_{K} \boldsymbol{\Lambda}_{m}^{(\mathsf{tx})} \boldsymbol{F}_{K}^{H}, \ \boldsymbol{\Lambda}_{m}^{(\mathsf{tx})} = \operatorname{diag} \left\{ \left[\boldsymbol{W}_{\mathsf{tx}} \right]_{(:,m)} \right\}.$$
 (20)

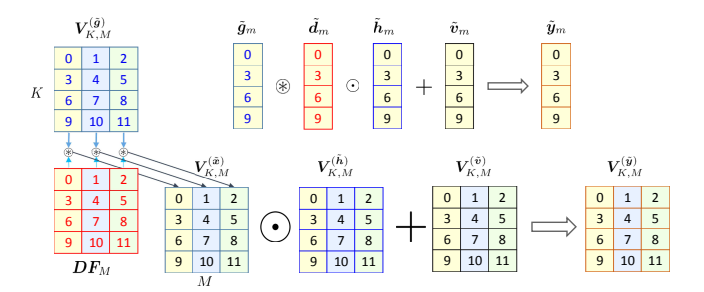


Fig. 3: Parallel signal model.

Considering full allocation, uncorrelated data, and uncorrelated noise, then $\mathrm{E}\left[\tilde{\boldsymbol{d}}_{m}\tilde{\boldsymbol{d}}_{m}^{H}\right]=ME_{s}\boldsymbol{I}_{K}$ and $\mathrm{E}\left[\tilde{\boldsymbol{d}}_{m}\tilde{\boldsymbol{d}}_{p}^{H}\right]=\boldsymbol{0}_{K},p\neq m.$ Therefore, $\mathrm{E}\left[\tilde{\boldsymbol{y}}_{m}\tilde{\boldsymbol{y}}_{p}^{H}\right]=\boldsymbol{0}_{K},p\neq m.$ This means that the received signal can be decoupled into M parallel uncorrelated signals, each has the size of K samples.

A. LMMSE-CEq

The LMMSE CEq can be performed on the signal (19). Let $\tilde{H}_{m,\text{eq}}^H$ be the channel equalizer given by

$$\tilde{\boldsymbol{H}}_{m,\text{eq}}^{H} = \left(\boldsymbol{\Lambda}_{m}^{(\tilde{h})}{}^{H}\boldsymbol{\Lambda}_{m}^{(\tilde{h})} + \tilde{\sigma}^{2}\boldsymbol{R}_{\bar{d},m}^{-1}\right)^{-1}\boldsymbol{\Lambda}_{m}^{(\tilde{h})}{}^{H}, \tag{21}$$

where $R_{\bar{d},m} = ME_s \tilde{A}_m \tilde{A}_m^H = \frac{ME_s}{K} F_K \Lambda_m^{(tx)} \Lambda_m^{(tx)} F_K^H$. If the elements of $\Lambda_m^{(tx)}$ are of equal amplitude then $R_{\bar{d},m}$ is diagonal and thus $\tilde{H}_{m,eq}^H$ is diagonal. For instance, in conventional GFDM with two subcarrier overlap, depending on the roll-off factor, there is several indexes where $\Lambda_m^{(tx)}$ satisfies the equal amplitude condition [11]. Otherwise, a practical LMMSE under diagonal matrix constraint is obtained using $\{R_{\bar{d},m}\}=\frac{ME_s}{K}P_m^{(tx)}I_K$, where

$$P_m^{(\text{tx})} = \text{trace}\left\{\boldsymbol{\Lambda}_m^{(\text{tx})}\boldsymbol{\Lambda}_m^{(\text{tx})H}\right\}. \tag{22}$$

Then,
$$\Lambda_{m,\text{eq}}^{(\tilde{h})} = \left(\Lambda_m^{(\tilde{h})}^H \Lambda_m^{(\tilde{h})} + \frac{K\tilde{\sigma}^2}{ME_s P_m^{(\text{tx})}} I_K\right)^{-1} \Lambda_m^{(\tilde{h})}^H$$
. (23)

The implementation of this receiver requires the knowledge of P_m , which can be acquired in advance. The inverse is realized with a real-valued reciprocal block. In addition, one block to compute the absolute value and a complex multiplier are required to compute the CEq.

B. LMMSE-GFDM-demodulation

After applying ZF-CEq on (19), we get

$$\tilde{\mathbf{y}}_{\text{eq},m} = \frac{1}{K} \mathbf{F}_K \mathbf{\Lambda}_m^{(\text{tx})} \mathbf{F}_K^H \tilde{\mathbf{d}}_m + {\mathbf{\Lambda}_m^{(\tilde{h})}}^{-1} \tilde{\mathbf{v}}_m. \tag{24}$$

The next step of the modulator is to apply K-IDFT,

$$\frac{1}{K} \boldsymbol{F}_{K}^{H} \tilde{\boldsymbol{y}}_{\text{eq},m} = \frac{1}{K} \boldsymbol{\Lambda}_{m}^{(\text{tx})} \boldsymbol{F}_{K}^{H} \tilde{\boldsymbol{d}}_{m} + \frac{1}{K} \boldsymbol{F}_{K}^{H} \boldsymbol{\Lambda}_{m}^{(\tilde{h})^{-1}} \tilde{\boldsymbol{v}}_{m}. \tag{25}$$

The LMMSE window can then be computed as

$$\mathbf{\Gamma}_{m}^{(\mathrm{rx})} = \mathbf{\Lambda}_{m}^{(\mathrm{tx})H} \left(\mathbf{\Lambda}_{m}^{(\mathrm{tx})} \mathbf{\Lambda}_{m}^{(\mathrm{tx})H} + \frac{K}{ME_{s}} \mathbf{R}_{v_{s},m} \right)^{-1}, \quad (26)$$

where
$$\mathbf{R}_{d_s,m} = \frac{ME_s}{K} \mathbf{I}_K$$
, $\mathbf{R}_{v_s,m} = \frac{\tilde{\sigma}^2}{K^2} \mathbf{F}_K^H \left[\mathbf{\Lambda}_m^{(\tilde{h})} \mathbf{\Lambda}_m^{(\tilde{h})}^H \right]^{-1} \mathbf{F}_K$.

In general $\Gamma_m^{(rx)}$ is not diagonal. To allow GFDM demodulation, we consider the constraint of diagonal matrix, which is achieved by using diag $\{\mathbf{R}_{v_s,m}\} = \frac{\tilde{\sigma}^2}{K^2} \Omega_m^{(\tilde{h})} \mathbf{I}_K$, where

$$\Omega_m^{(\tilde{h})} = \operatorname{trace} \left\{ \left[\mathbf{\Lambda}_m^{(\tilde{h})} \mathbf{\Lambda}_m^{(\tilde{h})}^H \right]^{-1} \right\}. \tag{27}$$

Thus,
$$\mathbf{\Lambda}_{m}^{(\mathrm{rx})} = \mathbf{\Lambda}_{m}^{(\mathrm{tx})H} \left(\mathbf{\Lambda}_{m}^{(\mathrm{tx})} \mathbf{\Lambda}_{m}^{(\mathrm{tx})H} + \frac{\tilde{\sigma}^{2} \Omega_{m}^{(\tilde{h})}}{E_{s} N} \mathbf{I}_{K} \right)^{-1}$$
. (28)

Thus, $[W_{\rm rx}]_{(k,m)} = \left[\Lambda_m^{(\rm rx)}\right]_{(k,k)}$. For each frame, the receiver window needs to be updated based on the channel coefficients. First $\{\Omega_m^{(\tilde{h})}\}$ are computed along the ZF-CEq. Assuming the absolute values of $\left[\Lambda_m^{(\rm rx)}\right]_{(k,k)}$ are stored in advance, only a real-valued reciprocal block and additional complex multiplier are required to compute the window.

C. SNR analysis

Assume a CEq matrix $\tilde{\boldsymbol{H}}_{m,\text{eq}}^{H}$ and demodulation matrix $\tilde{\boldsymbol{B}}_{m}^{H} = \frac{1}{K} \boldsymbol{F}_{K} \boldsymbol{\Lambda}_{m}^{(\text{rx})} \boldsymbol{F}_{K}^{H}$. After performing CEq and the demodulator convolution, as shown in Fig. 1, we get the estimate

$$\hat{\tilde{\boldsymbol{d}}}_{m} = \underbrace{\tilde{\boldsymbol{B}}_{m}^{H} \tilde{\boldsymbol{H}}_{m,eq}^{H} \boldsymbol{\Lambda}_{m}^{(\tilde{\boldsymbol{h}})} \tilde{\boldsymbol{A}}_{m}}_{\tilde{\boldsymbol{C}}_{m}} \tilde{\boldsymbol{d}}_{m} + \underbrace{\tilde{\boldsymbol{B}}_{m}^{H} \tilde{\boldsymbol{H}}_{m,eq}^{H}}_{\tilde{\boldsymbol{E}}_{m}} \tilde{\boldsymbol{v}}_{m}. \tag{29}$$

Following the remaining demodulator steps, namely, transpose then M-IDFT, we get the (k, m)-th estimated symbol as

$$\hat{d}_{k,m} = A_{k,m} d_{k,m} + \bar{z}_{k,m} + \bar{v}_{k,m}, \tag{30}$$

where $A_{k,m}$ is the overall gain, $\bar{z}_{k,m}$ is the ISI due to the final M-IDFT, and $\bar{v}_{k,m}$ is the sum of the ICI resulting from CEq and additive noise. The related power equations are

$$A_{k,m} = \frac{1}{M} \sum_{m=0}^{M-1} \left[\tilde{C}_m \right]_{(k,k)}, \ P_{k,m} = E_s |A_{k,m}|^2,$$
 (31)

$$I_{k,m}^{\text{ISI}} = \mathrm{E}\left[\left|\bar{z}_{k,m}\right|^{2}\right] = \frac{E_{s}}{M} \sum_{m=0}^{M-1} \left|\left[\tilde{C}_{m}\right]_{(k,k)}\right|^{2} - P_{k,m}.$$
 (32)

$$\operatorname{E}\left[\left|\bar{v}_{k,m}\right|^{2}\right] = \underbrace{\frac{E_{s}}{M} \sum_{m=0}^{M-1} \sum_{q=0, q \neq k}^{K-1} \left|\left[\tilde{C}_{m}\right]_{(k,q)}\right|^{2}}_{I_{k,m}^{\text{ICI}}, \text{ ICI power}} + \underbrace{\frac{\tilde{\sigma}^{2}}{M^{2}} \sum_{m=0}^{M-1} \sum_{q=0}^{K-1} \left|\left[\tilde{E}_{m}\right]_{(k,q)}\right|^{2}}_{\sigma_{k,m}^{2}, \text{ Noise power}}.$$
(33)

Thereby,
$$SINR_{k,m}(\boldsymbol{h}) = \frac{P_{k,m}}{I_{\cdot}^{ISI} + I_{\cdot}^{ICI} + \sigma_{i}^{2}}.$$
 (34)

Because $\mathrm{SINR}_{k,m}(h)$ is independent of m, all the subsymbols in the same subcarrier have an equal SINR. A low complexity computation of the SINRs values is achieved by exploiting the circular matrices $\{\tilde{A}_m\}$ and $\{\tilde{B}_m\}$ used to compute $\{C_m\}$ and $\{E_m\}$, especially for the practical diagonal CEq.

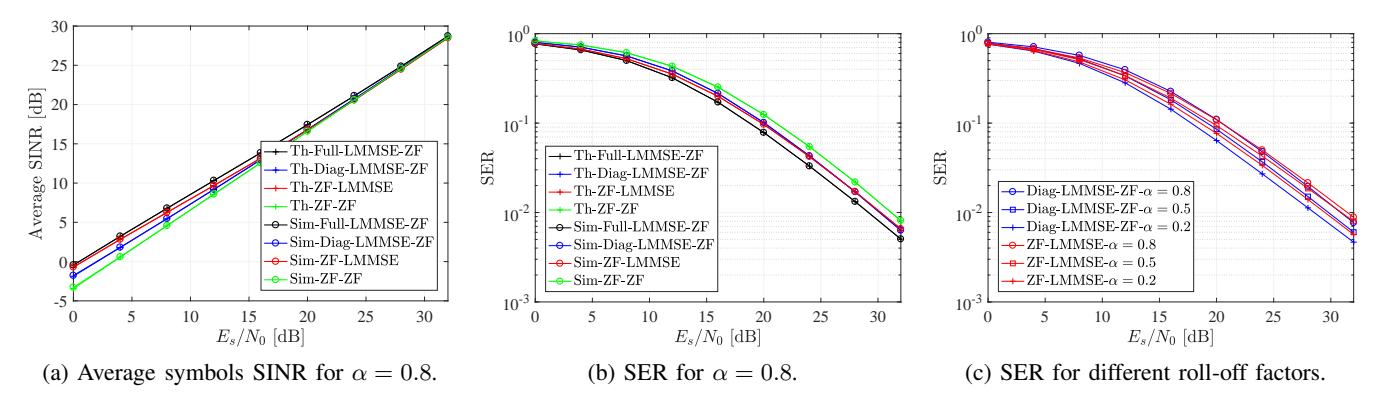


Fig. 4: Evaluation of non-orthogonal conventional GFDM in block fading channel of exponential PDP.

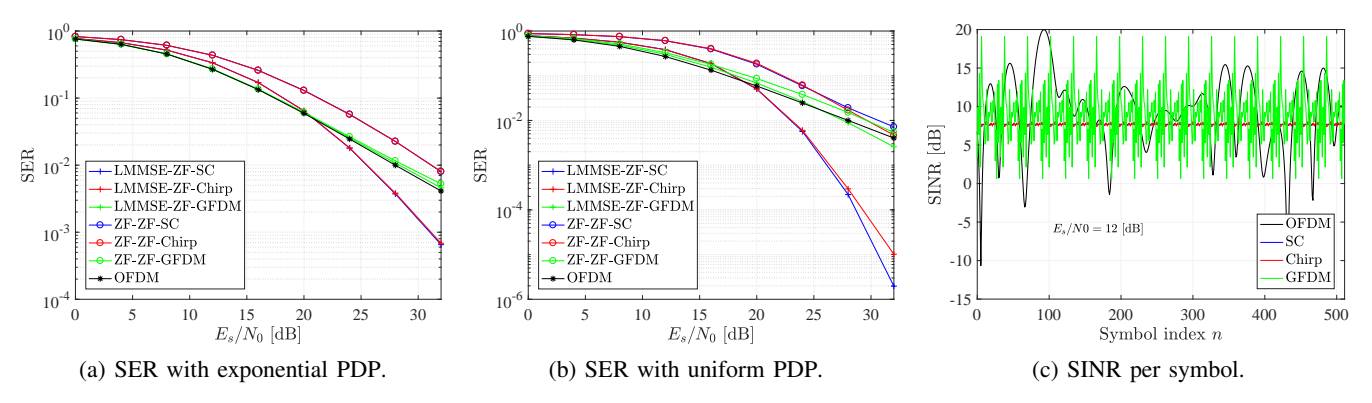


Fig. 5: Evaluation of orthogonal GFDM-based waveforms.

V. EVALUATION

In this section, we evaluate the performance of the typical GFDM-based (CEq-Demodulation) receivers in terms of symbol error rate (SER)¹ for conventional non-orthogonal GFDM design and other orthogonal designs based on GFDM.

A. Configurations

The conventional non-orthogonal GFDM is designed with a periodic raised-cosine (RC) prototype pulse shape with roll-off factor $0<\alpha<1,\ M\alpha>1,\ [11].$ The orthogonal case of GFDM ($\alpha=0$) is compared with other orthogonal GFDM-based waveforms of the same block length. Namely, OFDM, single carrier (SC) and Chirp-based. The configuration parameters are listed in Table I. We assume the channel

TABLE I: Modem parameters.

	K	M	Prototype pulse
GFDM	32	16	periodic RC (α)
OFDM	512	1	rectangular TD pulse
SC	1	512	rectangular FD pulse
Chirp	32	16	$g[n] = \left\{ \begin{array}{ll} e^{j\pi \frac{n^2}{K}} & , 0 \le n < K \\ 0 & , K \le n < N \end{array} \right\}$

impulse response is represented with L=24 uncorrelated taps

of zero-mean circular symmetric complex Gaussian (ZMCSC) distribution with exponential or uniform power-delay-profile (PDP). The data symbols are selected from $(M_c=16)$ -QAM constellation with uniform distribution and mean power E_s . The AWGN has the variance N_0 and the average signal-tonoise ratio (SNR) is defined by the ratio E_s/N_0 . The (k,m)-th SER for a given channel realization h is given by h

$$\operatorname{SER}_{k,m}(\boldsymbol{h}) = 1 - \left[1 - 2\frac{\sqrt{M_c}-1}{\sqrt{M_c}}Q\left(\sqrt{\frac{3\operatorname{SNR}_{k,m}(\boldsymbol{h})}{M_c-1}}\right)\right]^2$$
. The SER is computed by averaging over all symbols and channel realizations.

B. Non-orthogonal design

The possible CEq options include Full-LMMSE (21), Diag-LMMSE (23), and ZF. The demodulation follows the LMMSE design (28) or can be ZF. The joint LMMSE is achieved with the receiver Full-LMMSE-ZF. In Fig. 4a and Fig. 4b, we verify the closed-form computation of the per-symbol SINR (32) via numerical simulation by illustrating the average SINR and SER over different channel realizations, respectively. Further, it can be shown that the approximation of joint LMMSE outperforms the simple ZF receiver. For this particular design, performing ZF-CEq first approaches the joint LMMSE for lower SNRs. However, when the modulation matrix is well-conditioned, which can be achieved with smaller roll-off factor, the performance of ZF-LMMSE becomes worse

¹The goal of this simulation is to validate the concept of GFDM-based receiver. For realistic performance evaluation, coded BER should be considered.

 $^{^2}ar{z}_{k,m}+ar{v}_{k,m}$ in (30) is Gaussian according to central limit theorem.

than performing diagonal LMMSE-CEq first, as shown in Fig. 4c. Actually, for $\alpha=0.2$, the modulation window contains more equal-amplitude columns, as discussed in Section IV-B. Therefore, the receiver Diag-LMMSE-ZF is a good approximation of the joint LMMSE. In this context, a hybrid design of the equalizer and the demodulator can be used depending on the m-th column of the transmit window. If this has equal-amplitude values, an exact diagonal LMMSE equalizer is achieved and thus, the corresponding column of the demodulator window is chosen as ZF. In the other case, ZF equalization and then LMMSE design of the demodulator window is used. On the other hand, it can be seen from Fig. 4c that the SER decreases with the decrease of α , i.e. when the modulation tends to be more orthogonal.

C. Orthogonal design

In this section, we compare different orthogonal waveforms with the conventional GFDM ($\alpha = 0$). The optimal joint LMMSE is achieved via the diagonal LMMSE-CEq followed by ZF-demodulation. Fig. 5a demonstrates the SER for different orthogonal design with exponential PDP. In OFDM, the data symbols are transmitted over narrow subcarriers, and in GFDM over larger subcarriers, whereas in SC and chirp-based, they are spread over the whole band. The spreading allows higher frequency diversity, which is observed by the decreased SER at higher SNRs. This gain can be significantly observed with uniform PDP, as depicted in Fig. 5b. The gap between ZF and LMMSE is larger in the spreading case. Furthermore, a slightly better performance of GFDM is observed compared to OFDM. This is because the symbols are spread on wider subcarriers than that of OFDM. As a result, the variation in the symbol's SINR is smaller. The equal SINR per symbols is attained with SC for a given channel realization, as illustrated in Fig. 5c. The Chirp-based has a slight variation, whereas OFDM suffers from a significant variation in the SINRs.

VI. CONCLUSION

In this work, we consider GFDM as a multicarrier framework to process different waveforms. For practical implementation, the GFDM-based receiver is decoupled into channel equalization (CEq) and demodulation. The LMMSE-CEq under diagonal constraint followed by ZF-demodulation achieves better performance than the simple ZF receiver. Moreover, it approaches the performance of optimal joint LMMSE for non-orthogonal GFDM waveform and it becomes exact for orthogonal designs. The alternative ZF-CEq followed by LMMSE-GFDM demodulation is more appropriate when the self-interference due to non-orthogonality is higher. Thereby, a hybrid design of the equalizer and the demodulator can benefit from the structure of the modulator window. The complexity of the receiver is actually influenced by the non-orthogonality of the modulation. However, the performance in terms of SER tends to improve when the self-interference is reduced. Thus, the orthogonal modulation achieves better performance with low complexity implementation. Considering orthogonal design, we show that spreading the data symbols over wider

subcarriers enables frequency diversity. Accordingly, in block fading frequency selective channels, single carrier (SC) and Chirp-based GFDM with spreading over the whole bandwidth can achieve very low BER employing without channel coding. Additionally, the conventional GFDM with wider subcarrier spacing can outperform OFDM in certain channels.

REFERENCES

- [1] N. Michailow et al., "Generalized Frequency Division Multiplexing for 5th Generation Cellular Networks," *IEEE Trans. Commun.*, vol. 62, no. 9, pp. 3045–3061, Sep. 2014.
- [2] M. Danneberg et al., "Universal waveforms processor," in IEEE EuCNC, 2018, pp. 357–362.
- [3] —, "Flexible GFDM implementation in FPGA with support to runtime reconfiguration," in *IEEE VTC Fall*, 2015, pp. 1–2.
- [4] A. Farhang et al., "Low complexity GFDM receiver design: A new approach," in IEEE ICC, London, UK, June 2015, pp. 4775–4780.
- [5] A. Nimr et al., "A study on the physical layer performance of GFDM for high throughput wireless communication," in *IEEE EUSIPCO*, 2017, pp. 638–642.
- [6] I. Gaspar et al., "Low Complexity GFDM Receiver Based on Sparse Frequency Domain Processing," in *IEEE VTC Spring*, June 2013, pp. 1–6
- [7] M. Matthe et al., "Reduced complexity calculation of LMMSE filter coefficients for GFDM," in IEEE VTC Fall, Sept 2015, pp. 1–2.
- [8] P. Chen et al., "Matrix Characterization for GFDM: Low Complexity MMSE Receivers and Optimal Filters," IEEE Trans. Signal Process., vol. 65, no. 18, pp. 4940–4955, Sept 2017.
- [9] S. Tiwari and S. S. Das, "Low-Complexity Joint-MMSE GFDM Receiver," *IEEE Trans. Commun.*, vol. 66, no. 4, pp. 1661–1674, April 2018
- [10] D. Carrillo et al., "Bit Error Probability for MMSE Receiver in GFDM Systems," *IEEE Commun. Lett.*, vol. 22, no. 5, pp. 942–945, May 2018.
- [11] A. Nimr et al., "Optimal Radix-2 FFT Compatible Filters for GFDM," IEEE Commun. Lett., vol. 21, no. 7, pp. 1497–1500, 2017.
- [12] S. M. Kay, "Fundamentals of statistical signal processing, volume i: Estimation theory (v. 1)," PTR Prentice-Hall, Englewood Cliffs, 1993.

APPENDIX

A. Proof of Lemma 1

For a general linear model y = Gd + v, the LMMSE [12] receiver matrix can be expressed in two forms as

$$W^{H} = R_{d}G^{H} \left(GR_{d}G^{H} + R_{v}\right)^{-1}$$

$$= \left(G^{H}R_{v}^{-1}G + R_{d}^{-1}\right)^{-1}G^{H}R_{v}^{-1}.$$
(35)

Let G = HA, $R_d = E_s I_N$, and $R_v = \sigma^2 I_N$, the LMMSE using the first line of (35) is given by

$$\boldsymbol{W}^{H} = \underbrace{E_{s}\boldsymbol{A}^{H} \left(E_{s}\boldsymbol{A}\boldsymbol{A}^{H} + \sigma^{2}\boldsymbol{H}^{-1}\boldsymbol{H}^{H^{-1}}\right)^{-1}}_{\boldsymbol{B}_{\text{LMMSE}}^{H}} \boldsymbol{H}^{-1}.$$

Noting that, $\sigma^2 \boldsymbol{H}^{-1} \boldsymbol{H}^{H^{-1}} = \mathrm{E}\left[\bar{\boldsymbol{v}}\bar{\boldsymbol{v}}^H\right]$, $\bar{\boldsymbol{v}} = \boldsymbol{H}^{-1}\boldsymbol{v}$. Then, $\boldsymbol{B}_{\mathrm{MMSE}}^H$ is the LMMSE demodulation matrix with respect to $\boldsymbol{y}_{\mathrm{zf}} = \boldsymbol{A}\boldsymbol{d} + \bar{\boldsymbol{v}}$. As a result, $\hat{\boldsymbol{d}} = \boldsymbol{W}^H \boldsymbol{y} = \boldsymbol{B}_{\mathrm{LMMSE}}^H \left[\boldsymbol{H}^{-1}\boldsymbol{y}\right]$. On the other hand, by using the second line of (35)

$$oldsymbol{W}^H = oldsymbol{A}^{-1} \underbrace{\left(rac{1}{\sigma^2} oldsymbol{H}^H oldsymbol{H} + [E_s oldsymbol{A} oldsymbol{A}^H]^{-1}}^{-1} oldsymbol{H}^H rac{1}{\sigma^2}.$$

Here, $E_s A A^H = E[\bar{d}\bar{d}^H]$, $\bar{d} = Ad$. Thus, H_{LMMSE} is the LMMSE channel equalization with respect to $y = H\bar{d} + v$. Accordingly, $\hat{d} = W^H y = A^{-1}[H_{\text{LMMSE}} y]$.